Results in Physics 44 (2023) 106182

Contents lists available at ScienceDirect

Results in Physics

journal homepage: www.elsevier.com/locate/rinp

Effects of the confinement potential parameters and optical intensity on the linear and nonlinear optical properties of spherical quantum dots

C.O. Edet [a,b,c,*], E.B. Al [d], F. Ungan [d], N. Ali [b,e,*], M.M. Ramli [f,g], M. Asjad [h,**]

[a] Institute of Engineering Mathematics, Universiti Malaysia Perlis, 02600 Arau, Perlis, Malaysia
[b] Faculty of Electronic Engineering Technology, Universiti Malaysia Perlis, Malaysia
[c] Department of Physics, Cross River University of Technology, Calabar, Nigeria
[d] Physics Department, Faculty of Science, Sivas Cumhuriyet University, 58140 Sivas, Turkey
[e] Advanced Communication Engineering (ACE) Centre of Excellence, Universiti Malaysia Perlis, 01000 Kangar, Perlis, Malaysia
[f] Institute of Nano Electronic Engineering (INEE), Universiti Malaysia Perlis (UniMAP), 01000 Kangar, Perlis, Malaysia
[g] Geopolymer & Green Technology, Centre of Excellence (CEGeoGTech), Universiti Malaysia Perlis (UniMAP), Perlis, Malaysia
[h] Department of Mathematics, Khalifa University, Abu Dhabi 127788, United Arab Emirates

ARTICLE INFO

Keywords:
Schrödinger equation
Screened modified Kratzer potential (SMKP)
Refractive index
Absorption coefficient
Optical transitions
Diagonalization method

ABSTRACT

We study the linear and nonlinear optical properties of a spherical GaAs quantum dot with screened modified Kratzer potential (SMKP) by solving the time-independent Schrödinger wave equation using the diagonalization method. The obtained electronic properties of the system alongside the compact density formalism are used to evaluate the linear, third-order nonlinear and total optical absorption coefficients and change in the relative refractive index of the system. We show that the confinement potential parameters and optical intensity significantly affects the behaviour of absorption coefficients and refractive index changes. It is important to note that the findings of this study will find application in optoelectronics and related areas.

Introduction

Due to the massive increase in research focusing on the physics of low-dimensional semiconductor nanostructures in the last three decades, there have been remarkable developments in this area [1–5]. Such studies have been inspired by the urgent need for advanced nano-fabricated technologies. Semiconductor nanostructures are manufactured using sophisticated growth methods like *chemical lithography* and *molecular-beam epitaxy* [6–8]. Examples of these structures are superlattices, quantum wires, single and multiple quantum wells, pseudo dot and quantum dots (QDs), antidots, antiwells, etc. [9–15]. The aforementioned structures have received unprecedented attention from both theorists and experimentalists [16–19]. These structures have great potential in device applications such as laser, optical modulation technology, etc.[20,21]. Several researchers have studied the properties of these structures via the experimental approach [22,23]. Furthermore, numerous theoretical investigations have been carried out with these structures such as band structure calculations, optical properties, transport properties and polaron effects, etc [24–28].

Research on optical properties of low-dimensional structures, finds direct applications in design of electronic devices such as laser diodes. Consequently, optical properties of semiconductor heterostructures have attracted significant attention [29–31]. The confinement geometry in low-dimensional structures hinders the flow of charge carriers in space, and as a result of the discrete electronic energy distribution, the behaviour in the electrical and optical properties of such systems changes. Because of the above-mentioned, energy levels and wave functions are two of the major electronic properties that can be used theoretically to determine the optical properties of zero-dimensional structures [29–31]. In the past decade, several studies have been carried out on the electronic, thermal and optical properties of quantum wires with various cross-sections [25,26,31,32]. The attention of the researchers was attracted by the fact that these electronic properties provide information about the optical properties of the system, such as the optical absorption coefficient and refractive index [33–40]. Consequently, many optical properties of semiconductor QDs such as dipole transition [24,25], oscillator strength [26,27], photoionization cross-sections [28], optical absorption coefficients (OACs) [31] and refractive index changes (RICs) [26] have appealed the interest of scholars in experimental and theoretical studies in recent years [28,33–35].

The electronic and optical properties of QDs have been investigated using various models such as Tietz [36], Gaussian [37], modified Gaussian [38], modified Kratzer [39], Rosen–Morse [40], Manning–Rosen [41] and inversely quadratic Hellmann potential [31]. However,

* Corresponding authors at: Faculty of Electronic Engineering Technology, Universiti Malaysia Perlis, Malaysia.
** Corresponding author.
E-mail addresses: collinsokonedet@gmail.com (C.O. Edet), norshamsuri@unimap.edu.my (N. Ali), muhammad.asjad@ku.ac.ae (M. Asjad).

https://doi.org/10.1016/j.rinp.2022.106182
Received 17 June 2022; Received in revised form 6 December 2022; Accepted 13 December 2022
Available online 15 December 2022

to the best of our knowledge, the optical properties of QDs have not been studied using the screened modified Kratzer potential (SMKP), which is given as [42–44]:

$$V_S(r) = D_e\left(q - \frac{r_e}{r}e^{-\alpha r}\right)^2, \tag{1}$$

where D_e is the dissociation energy, r_e is the equilibrium bond length, α is the screening parameter, q is the control parameter and r is the internuclear distance. This SMKP has been applied by several authors to study diatomic molecules and other physical systems [45–51]. Moreover, our choice is inspired by the fact that potential models with many fitting parameters tend to study physical systems and/or fit experimental data better than ones with fewer parameters.

In view of the details highlighted above, it is clear that the relevant motive for the present study is established. Being relevant to the field of device applications, the QDs are systems that exhibit remarkable optical and electronic properties. These can be properly tuned by suitably modifying the composition, structural parameters, and the application of external probes. Here, the linear and nonlinear optical properties of a spherical GaAs QD structure with SMKP confinement potential have been investigated. Thereafter, the effects of the multiple confinement potential parameters on the coefficients of linear and nonlinear optical absorption and refractive index change will be separately scrutinized. The organization of the article is as follows: in section "Theory", the formulation and theoretical solution of the problem are given, theoretical details of optical properties is presented in Section "Optical properties: theoretical details", numerical results and their discussions are presented in Section "Results and Discussions" and our conclusions are given in Section "Conclusion".

Theory

In the framework of the effective mass approach, the Schrödinger equation in spherical coordinates for a spherical QD can be expressed as

$$\left[\frac{\vec{p}^{\,2}}{2m^*} + V_S(r)\right]\psi_{nlm}(r,\theta,\phi) = E_{nlm}\psi_{nlm}(r,\theta,\phi), \tag{2}$$

where, $\vec{p}$ and m^* are the linear momentum vector and the effective mass of the electron, n, l and m are principal, orbital and magnetic quantum numbers, and $V_S(r)$ is the screened modified Kratzer potential. The wavefunction-$\psi_{nlm}(r,\theta,\phi)$ in the Eq. (2) can be found by a series expansion using well-known wavefunctions as a basis [31]:

$$\psi_{nlm}(r,\theta,\phi) = \sum_j c_{n_j l_j m}\psi^{(0)}_{n_j l_j m}(r,\theta,\phi). \tag{3}$$

where c_{nlm} are the expansion coefficients, $\psi^{(0)}_{nlm}(r,\theta,\phi)$ is the total wave function describing the motion of the electron and the exact solution for an electron in a spherical QD with infinite potential is [31]

$$\psi^{(0)}_{nlm}(r,\theta,\phi) = \varphi^{(0)}_{nl}(r)Y_{lm}(\theta,\phi), \tag{4}$$

where the radial wavefunction-$\varphi^{(0)}_{nl}(r)$ is given as

$$\varphi^{(0)}_{nl}(r) = \begin{cases} N j_l(k_{nl}r), & r < a \\ 0, & r \geq a \end{cases}, \tag{5}$$

where N is the normalization constant, k_{nl} is the nth root of the spherical Bessel function-j_l and $a = 55$ nm is the radius of the infinite spherical QD. It should be noted that we do the series expansion only for $m = 0$ states.

Optical properties: theoretical details

This section focuses on the application of the well-known compact density matrix formalism to compute the variations in absorption coefficients and refractive index-linked to optical transitions involving two sub-bands [31,32,36,37]. The ground and first excited state energy levels of the QD used in the calculations represent the subbands E_1 and E_2. Optical absorption occurs when the incident photon energy-$\hbar\omega$ equals the energy difference between the subbands ($\hbar\omega = E_{21} = E_2 - E_1$) [40]. In this case, with the absorption of the photon, an electron transitions from the ground to the excited states. This process, called photoabsorption, is highly dependent on the photon's energy and QD parameters. The incident photons is created by an electromagnetic (EM) radiation which is polarized in the z-direction. Incident photons are generated by electromagnetic (EM) radiation that is polarized in the z-direction [31]. This EM field is considered as $E(t) = E_0\cos(\omega t) = \bar{E}e^{i\omega t} + \bar{E}^*e^{-i\omega t}$, where $\bar{E}$ and ω are the amplitude and the angular frequency of the electric field, respectively [34,35]. The time evolution of the matrix elements is evaluated in the case of one-electron density operator ρ [31,32,36–39],

$$\frac{\partial\rho}{\partial t} = \frac{1}{i\hbar}[H_0 - ezE(t), \rho] - \Gamma(\rho - \rho^{(0)}), \tag{6}$$

where H_0 is the unperturbed Hamiltonian devoid of EM, $E(t)$ is the term containing perturbations, e is the charge of the electron, $\rho^{(0)}$ is the density matrix operator devoid of EM perturbations and Γ is a damping operator due to processes of collision [34]. Γ is adopted to be the diagonal matrix with elements equal to the inverse of the relaxation time τ [31,32]. The master Eq. (6) can be solved using an iterative procedure [31,32,36–41]: $\rho(t) = \sum_{n=0}^{\infty}\rho^{(n)}(t)$, where

$$\frac{\partial\rho^{(n+1)}_{ij}}{\partial t} = \frac{1}{i\hbar}[H_0, \rho^{(n+1)}]_{ij} - \frac{1}{i\hbar}[ez, \rho^{(n)}]_{ij}E(t) - \Gamma_{ij}\rho^{(n+1)}_{ij}. \tag{7}$$

Owing to the presence of the electric field, the electronic polarization is written in the form $P(t) = \varepsilon_0\chi(\omega)\bar{E}e^{-i\omega t} + \varepsilon_0\chi(-\omega)\bar{E}^*e^{i\omega t}$ and can be obtained from Eq. (6) as $P(t) = Tr(\rho M)/V$, where M is the dipole operator, $\chi(\omega)$ is the susceptibility, V is the volume and ε_0 is the permittivity of vacuum of the QD. In the serial expansion of the susceptibility $\chi(\omega)$ and taking into consideration the coefficients up to the third-order, the even orders of the susceptibility will be eliminated, by reason of the inversion symmetry of the QD [34]. After these calculations, the mathematical expressions of the linear $\chi^{(1)}(\omega)$ and the third-order nonlinear $\chi^{(3)}(\omega)$ susceptibility coefficients are presented as follows [31,32,36,37,39–41]:

$$\chi^{(1)}(\omega) = \frac{\sigma_v|M_{21}|^2}{\varepsilon_0 Y}, \tag{8}$$

$$\chi^{(3)}(\omega) = -\chi^{(1)}(\omega)|\bar{E}|^2\left[\frac{4|M_{21}|^2}{|Y|^2} - \frac{4|M_{22} - M_{21}|^2}{(E_{21} - i\hbar\Gamma_{12})Y}\right], \tag{9}$$

where $Y = E_{21} - \hbar\omega - i\hbar\Gamma_{12}$, $M_{ij} = \langle\psi_{n_i l_i m_i}|ez|\psi_{n_j l_j m_j}\rangle$ are the matrix elements of the electric dipole moment (m is the magnetic momentum quantum number), $E_{ij} = E_i - E_j$ is the energy difference between the two electronic states, $\hbar\omega$ is the incident photon energy and σ_v is the carrier density. The matrix elements of the electric dipole moment can be evaluated by:

$$M_{ij} = e\int r^3|\psi_{n_i l_i m_i}(r,\theta,\phi)|^2 dr\cos(\theta)\sin(\theta)d\theta d\phi, \tag{10}$$

where the $\psi_{n_i l_i m_i}(r,\theta,\phi)$ is the wave function.

The intersubband optical transition probability amplitude between the two electronic states, such as the lowest (initial) and the first excited (final), is proportional to the matrix element of electric dipole moment. Because the electric dipole moment is unaffected by spin, optical transitions can only occur between states with the same spin. When the selection rules $\Delta l = \pm 1$ and $\Delta m = 0$ are satisfied, the matrix elements of the electric dipole moment are non-vanishing [31,32]. The OAC-$\alpha(\omega)$ is gotten from the susceptibility-$\chi(\omega)$ using the relation given as $\alpha(\omega) = \omega\sqrt{\mu_0/\varepsilon}\,\Im m[\varepsilon_0\chi(\omega)]$ [31,32,36–41], where μ_0 is the vacuum permeability and $\varepsilon = n_r^2\varepsilon_0$ (where ε_0 and n_r are the permittivity and refractive index of the material, respectively). Then the linear and third-order nonlinear OACs can be expressed as

$$\alpha^{(1)}(\omega) = \omega\sqrt{\frac{\mu_0}{\epsilon}}\frac{\hbar\sigma_v\Gamma_{12}|M_{21}|^2}{|Y|^2}, \tag{11}$$

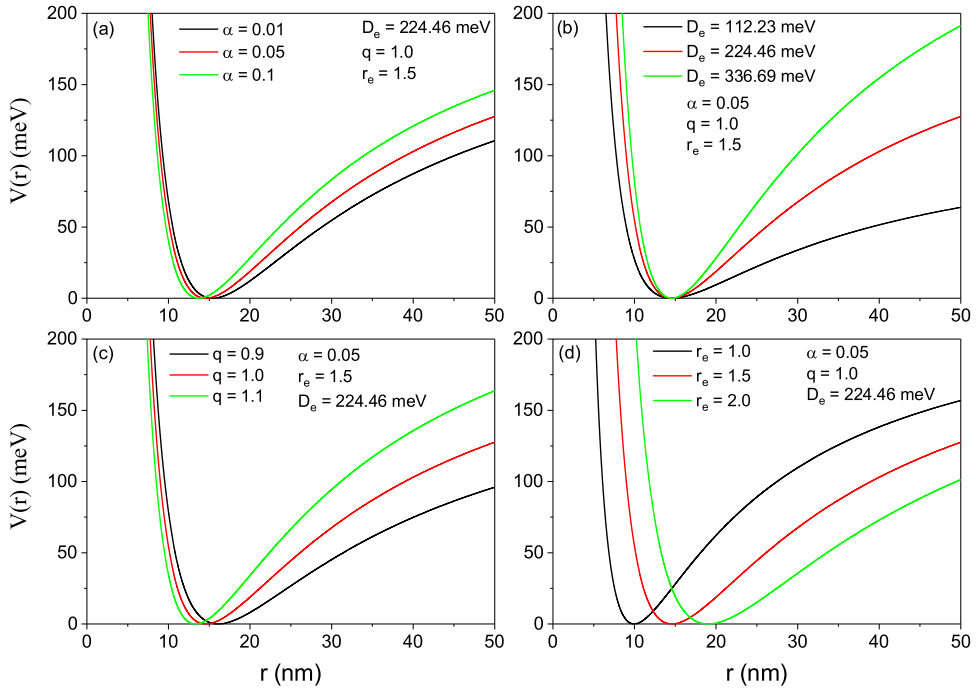

Fig. 1. The confining SMKP as a function of r for several values of the D_e, r_e, α and q.

$$\alpha^{(3)}(\omega, I) = -\omega I \sqrt{\frac{\mu_0}{\epsilon}} \frac{\hbar \sigma_v \Gamma_{12} |M_{21}|^2}{2\epsilon_0 n_r c} \left[\frac{4|M_{21}|^2}{\left(|Y|^2 - 2\hbar^2\Gamma_{12}^2\right)^2} - \frac{|M_{22} - M_{11}|^2 \left(2E_{21}(E_{21} - \hbar\omega) + |Y|^2 - 2\hbar^2\Gamma_{12}^2\right)}{\left(E_{21}^2 + \hbar^2\Gamma_{12}^2\right)\left(|Y|^2 - 2\hbar^2\Gamma_{12}^2\right)^2} \right], \tag{12}$$

where c is the speed of light in vacuum and $I = 2\epsilon_0 n_r c|\bar{E}|^2$ represents the incident optical intensity. The third-order nonlinear OAC- $\alpha^3(\omega, I)$ is negative and also it is proportional to the incident optical intensity-I. The total OAC is given by $\alpha(\omega, I) = \alpha^{(1)}(\omega) + \alpha^{(3)}(\omega, I)$ [31,32,36–41]. The susceptibility is linked to the RICs as $\Delta n(\omega)/n_r = \Re e[\chi(\omega)/2n_r^2]$ [32,41]. Then, the linear and third-order nonlinear RICs can be computed by using Eqs. (8) and (9):

$$\frac{\Delta n^{(1)}(\omega)}{n_r} = \frac{\sigma_v |M_{21}|^2}{2n_r^2\epsilon_0} \frac{E_{21} - \hbar\omega}{|Y|^2}, \tag{13}$$

$$I\frac{\Delta n^{(3)}(\omega, I)}{n_r} = \frac{\sigma_v |M_{21}|^2 \mu_0 c I}{4n_r^2\epsilon_0} \left\{ \frac{4(E_{21} - \hbar\omega)|M_{21}|^2}{(E_{21} - \hbar\omega)^2 - \hbar^2\Gamma_{12}^2} - \frac{|M_{22} - M_{11}|^2 \left[E_{21}(|Y|^2 - 4\hbar^2\Gamma_{12}^2) + 2\hbar\omega\Gamma_{12}^2\right]}{\left(|Y|^2 - 2\hbar^2\Gamma_{12}^2\right)|Y_{12}|^2} \right\}. \tag{14}$$

From above equations it is clear that the third-order nonlinear RIC- $\Delta n^{(3)}(\omega, I)/n_r$ has the opposite sign with the sign of $\Delta n^{(1)}(\omega)/n_r$ and it is proportionate to the incident optical intensity-I. Using Eqs. (13) and (14), the total RIC is given by $\Delta n(\omega)/n_r = \Delta n^{(1)}(\omega)/n_r + \Delta n^{(3)}(\omega, I)/n_r$. Therefore, it is clear form set of Eqs. (11)–(12) and Eqs. (13)–(14), the OACs and RICs, respectively, depends only on the matrix element M_{21} of the dipole moment. Once a photon with $\hbar\omega$ energy is released into the system, the matrix element-M_{21} provides the probability amplitude of an optical transition between the states $|1\rangle$ and $|2\rangle$ described by the wave functions $\psi_{n_1 l_1 m_1}$ and $\psi_{n_2 l_2 m_2}$, respectively.

Results and discussions

This study presents the optical properties of the GaAs QD structure with SMKP. Numerical computations are carried out for this QD structure. The fitting parameters used to achieve our set objectives are presented as follows: $\mu = 0.067me$, $\sigma_v = 2 \times 10^{22}$ m^{-3}, $n_r = 3.2$, $\epsilon_0 = 8.854 \times 10^{-12}$ F/m, $\mu_0 = 4\pi \times 10^{-7}$ H/m and $\Gamma_{12} = 1/\tau_{12}$ where $\tau_{12} = 0.14$ ps. The experimental values for the depth of the potential well-D_e and radius of the dot-$R_0 = 1/\alpha$ are selected in accordance with those obtained in the literature [31,39–41]. This dot radius helps to control the width of the potential well. The QD considered in this study was produced in a semiconductor heterostructure that comprises a 2D electron gas with lithographically attained metallic gate electrodes placed close to the QD. The energy levels and the size of the dot, e.g. the radius of the dot, can be changed by tuning the electrodes of the gate [39,40]. Computations are made in atomic units ($\hbar = m_e = e = 1$). The SMKP which has finite depth and range is the confining potential adopted for this study. This potential is a continuous function with four parameters that can be adjustable at will to fit a physical system of interest. In this study, our goal is to study the optical properties of a QD with SMKP. Historically, it has been established that for a potential model to be used to study intersubband transition occurrences and related properties of QDs, the potential must be in a quadratic-like form just like the SMKP (see Fig. 1). Fig. 1(a–d) shows the confining SMKP as a function of for several values of the D_e, r_e, α and q. As can be seen in these figures, an increase in the values of D_e, α and q parameters causes an increase in the finite part of the potential, while an increase in the r_e causes a decrease. Also, increasing of α and q parameters shifts the potential minimum to the smaller radial distance, while increasing of r_e shifts it to the larger radial distance. However, it is also seen that the change in D_e has no effect on the minimum of the potential. The shape of this model is in agreement with the shape of other confinement potentials previously adopted for such structures [32,36–41]. However, our model is an improvement to the aforementioned in the Ref. [39], in the sense that our potential has more fitting parameters and it is a general case of the Kratzer potential [39].

In Fig. 2 we show the OACs as a function of the photon energy for several values of D_e, r_e, α, and q. To study the OACs of this system, the incident optical intensity is fixed at $I = 400$ MW/m^2. It is observed from the Figs. 2 (a, b, c & d) that the linear and total OACs first increase and then decrease as the photon energy increases

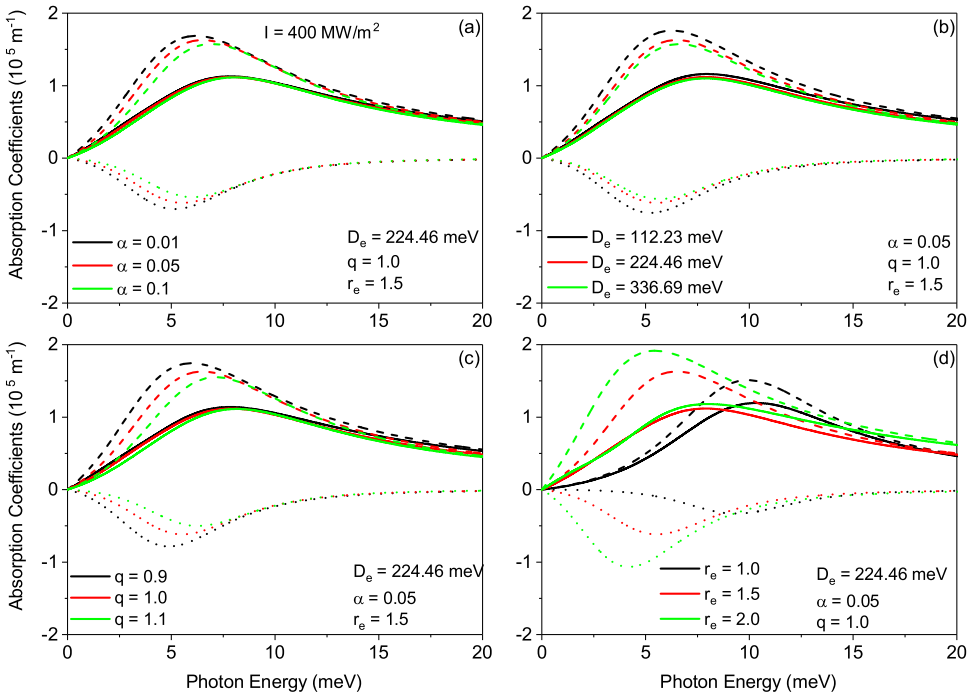

Fig. 2. The OACs as a function of the photon energy for several values of D_e, r_e, α and q. Dashed lines are for linear, dotted lines are for nonlinear and solid lines are for total OACs.

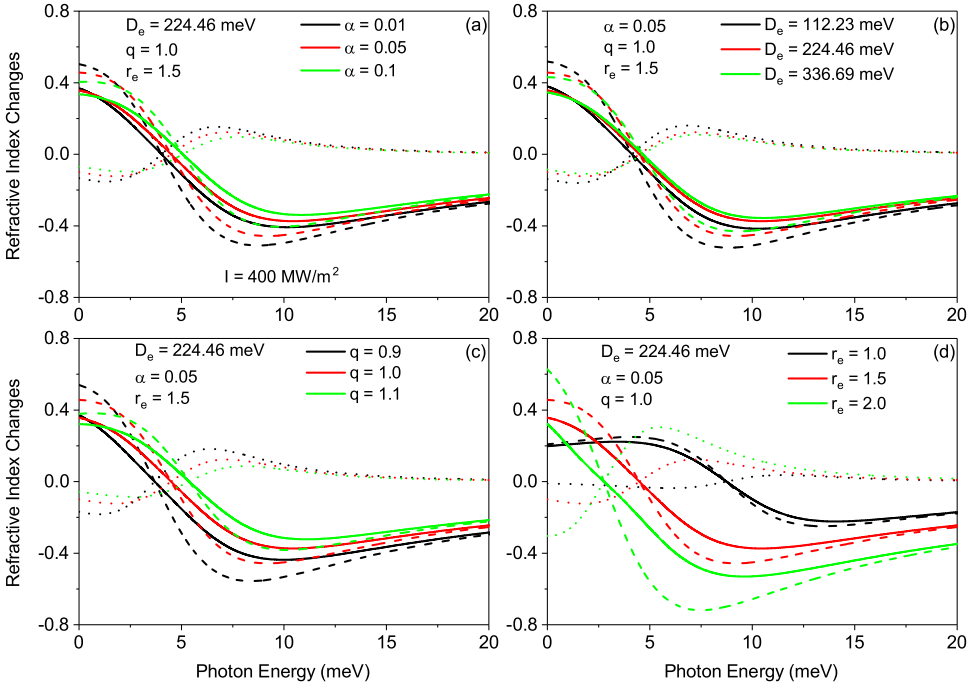

Fig. 3. The RICs as a function of the photon energy for several values of D_e, r_e, α and q. Dashed lines are for linear, dotted lines are for nonlinear and solid lines are for total RICs.

while negative nonlinear OAC shows the opposite change. A quasi-resonance peak is observed at a photon energy of ≈ 7.5 me V for total OAC. The increase in D_e, α and q parameters shifts the peak position of linear and nonlinear OACs slightly towards blue (high energy) due to the change in transition energy, while the increase in r_e causes these peaks to shift to red (low energy). In addition, the peak amplitudes of linear and nonlinear OACs decrease with the increasing of D_e, α and q parameters due to less overlapping of the wavefunctions of the ground and first excited states and hence the decrease of the dipole matrix element. On the other hand, with the increasing of r_e, the associated wave functions overlap more and accordingly, the peak amplitudes of linear and nonlinear OACs increase with the increasing of the dipole matrix element. However, there is no discernible difference on the total OAC with the variations of D_e, α and q except of r_e. As a result, we can conclude that although these parameters cause an effective change on linear and nonlinear OACs, their effect on the total OAC is very small.

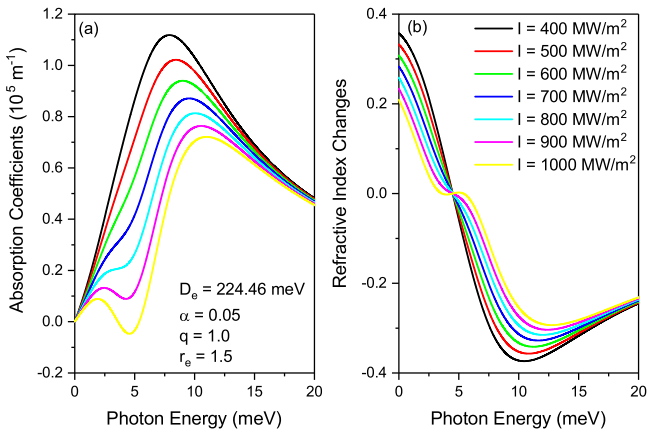

Fig. 4. (a) The total OAC as a function of the photon energy. (b) The total RICs as a function of the photon energy. Both plots are for several values of I and fixed D_e, r_e, α and q parameters.

In Fig. 3, we plot the RICs as a function of the photon energy for different values of D_e, r_e, α and q. With the rising of photon energy, the peak amplitude of the total RICs firstly decreases and then increases. In addition, as the D_e, α and q increase the peak position of the total RICs moves to the greater energies as shown in Fig. 3(a, b and c). This is attributed to the fact that the energy difference between the two electronic states increases as the D_e, α and q parameters increase. Fig. 3(d) shows the same behaviour for total RICs as the photon energy rises, but as the parameter r_e increases, the peak position of total RICs shifts to lower energies. This is because as the parameter r_e increases, the energy difference between the two electronic states decreases. Also, when D_e, α and q increase, the dipole matrix element and hence the peak amplitude of total RICs decrease, while the converse is seen as r_e increases.

Fig. 4(a) and (b) display the variations in the total OAC and RICs versus photon energy-$\hbar\omega$ for seven different incident optical intensity values with $\alpha = 0.05$, $r_e = 1.5$, $q = 1$ and $D_e = 224.46$ me V. As shown in Fig. 4(a), it is clearly seen that the amplitude of the total OAC decreases as the incident photon intensity rises. The underlying reason for this behaviour is that the third-order nonlinear OAC has a linear dependence on I, while the linear OAC is not dependent on it. Thus, as the intensity I increases, the peak amplitude of the total OAC decreases due to the negative contribution from the nonlinear OAC and the total OAC starts to quasi-saturate at the critical optical intensity-$I = 700$ MW/m^2 in the low photon energy regime. At the point where the magnitudes of the linear and nonlinear third-order OACs equal each other ($\alpha^{(1)} = |\alpha^{(3)}|$), the optical intensity is approximately $I = 1000$ MW/m^2, and at that point the OAC reaches zero. It is pertinent to note that if the optical intensity is raised beyond this point, this will produce negative values of the total OAC which is physically acceptable. In addition, it is interesting to note that the optical intensity does not affect the resonance peak position of the total OAC. Similarly, as stated earlier and it is clearly seen in Eq. (13) that there is no dependence of the linear RICs on the optical intensity. In consequence, the dependence of total RICs on optical intensity is gotten from the nonlinear third-order term which depends linearly on the optical intensity-I. It is shown that when the intensity rises, the amplitude of the total RICs alters. The linear term of RICs dominates for low optical intensities, but with the raising of the intensity, the impact of the nonlinear third-order term dominates. As a result, the nature of the total RIC varies accordingly. The results presented in this study agree excellently with earlier studies by other researchers using other models [31,32,34]. However, ours is an improvement because our model presents multiple parameters that can be utilized to tune and manipulate the properties of QDs.

Conclusion

This study theoretically investigates the linear, third-order nonlinear and total absorption coefficients and refractive index changes for spherical quantum dots. In this context, the screened modified Kratzer potential has been used. To derive the eigenvalues energies and wave functions, the Schrödinger equation in spherical coordinate was solved by applying the diagonalization method. The peak positions of the absorption coefficients and refractive index changes shift to blue or red upon the change of potential parameters. Furthermore, the resonance positions of the absorption coefficients and refractive index changes do not change by the optical intensity I, while their amplitudes change greatly. Our results are vital in the design of nano-scale electronic devices such as quantum dot solar cells, quantum dot lasers, quantum dot photodetectors, quantum dot infrared photodetectors, phototransistors, and light-emitting diodes.

CRediT authorship contribution statement

C.O. Edet: Conception and design of study, Acquisition of data, Analysis and/or interpretation of data, Handled the review. **E.B. Al:** Handled the computational analysis. **F. Ungan:** Conception and design of study, Acquisition of data, Analysis and/or interpretation of data, Handled the review. **N. Ali:** Writing – review & editing, Contributed in general recommendations and data interpretation. **M.M. Ramli:** Writing – review & editing, Contributed in general recommendations and data interpretation. **M. Asjad:** Writing – review & editing, Contributed in general recommendations and data interpretation.

Declaration of competing interest

The authors declare that they have no known competing financial interests or personal relationships that could have appeared to influence the work reported in this paper.

Data availability

Data will be made available on request.

Acknowledgements

This research has been carried out under LRGS Grant LRGS/1/2020/UM/01/5/2 (9012-00009) Fault-tolerant Photonic Quantum States for Quantum Key Distribution provided by Ministry of Higher Education of Malaysia (MOHE).

References

[1] Sandoval MT, La Rocca GC, Silva EDA. Phys E Low Dimens Syst Nanostruct 2022;138:115061.
[2] Ullah K, Meng Y, Shi Y, Wang F. Adv Opt Mater 2022;2:101860.
[3] Roudbari MA, Jorshari TD, Lu C, Ansari R, Kouzani AZ, Amabili M. Thin-Walled Struct 2022;170:108562.
[4] Yang M, Jin H, Sun Z, Gui R. J Mater Chem J Mater Chem A 2022;10:5111.
[5] Qi Y, Yang S, Wang J, Li L, Bai Z, Wang Y, et al. Mater Today Phys 2022;23:100622.
[6] Rotenberg E, Freelon BK, Koh H, Bostwick A, Rossnagel K, Schmid A, et al. New J Phys 2005;7:114.
[7] Gil AM, Rota A, Maroutian T, Bartenlian B, Beauvillain P, Moyen E, et al. Superlattices Microstruct 2004;36:235.
[8] Axelsson S, Campbell EEB, Jonsson LM, Kinaret J, Lee SW, Park YW, et al. New J Phys 2005;7:245.
[9] Cetin A. Phys Lett A 2008;372:3852.
[10] Aquino N, Castano E, Ley-Koo E. Chin J Physiol 2003;41:276.
[11] Bogachek EN, Landman U. Phys Rev B 1995;52:14067.
[12] Chepelianskii AD, Shepelyansky DL. Phys Rev B 2001;63:165310.
[13] Matulis A, Pyragiene T. Phys Rev B 2003;67:045318.
[14] Ikhdair S, Sever R. J Mol Struct 2007;806:155.
[15] Reijniers J, Peeters FM, Matilus A. Phys Rev B 1998;59:2817.
[16] Niley F, Nakamura K. Phys B 1993;184:398.

[17] Weiss D, Richiter K, Manschig A, Bergman R, Schweizer H, von Klitzing K. Phys Rev Lett 1993;70:4118.
[18] Chayanika B. J Appl Phys 1998;6:3089.
[19] Lisa K, Bednareka S, Szafrana B, Adamowski J. Phys E Low Dimens Syst Nanostruct 2003;17:494.
[20] Ijima S. Nature 1991;54:56.
[21] Kroto HW, O'Brein SR, Curl RF, Smalley RE. Nature 1985;318:162.
[22] Tanaka M, Yamada H, Maruyama T, Akimoto K. Phys Rev B 2003;67:045305.
[23] Rasanen E, Saarikoski H, Stavrou VN, Harju A, Puska MJ, Nieminen RM. Phys Rev B 2003;67:235307.
[24] Hasanirokh K, Asgari A, Rokhi MM. Optik 2019;188:99.
[25] Naimi Y. Chem Phys Lett 2021;767:138380.
[26] Shi L, Yan Z-W, Meng M-W. Superlattice Microst 2021;150:106818.
[27] Al EB, Kasapoglu E, Sari H, SoAl21kmen I. Phys B 2021;613:412874.
[28] Mgidlana S, P. Şen P, Nyokong T. J Mol Struct 2020;1220:128729.
[29] Perez-Conde J, Bhattacharjee AK. Solid State Commun 2005;135:496.
[30] Yakar Y, Çakır B, Özmen A. Superlattice Microst 2013;60:389.
[31] Al EB. Cumhuriyet Sci J 2021;42:694.
[32] Mathe L, Onyenegecha CP, Farcaş A-A, Pioraş-Ţimbolmaş L-M, Solaimani M, Hassanabadi H. Phys Lett 2021;397:127262.
[33] Mzerd S, El Haouari M, Talbi A, Feddi E, Mora-Ramos ME. J Alloy Comp 2018;753:68.
[34] Feddi E, Talbi A, Mora-Ramos ME, El Haouari M, Dujardin F, Duque CA. Phys B 2017;524:64.
[35] El Haouari M, Talbi A, Feddi E, El HG, Oukerroum A, Dujardin F. Opt Commun 2017;383:231.
[36] Khordad R, Mirhosseini B. Pramana 2015;85:723.
[37] Xie W. 48 (2010) 239.
[38] Gharaati A, Khordad R. 48 (2010) 276.
[39] Khordad R. Indian J Phys 2013;87:623, (2014).
[40] Khordad R, Mirhosseini B. Opt Spectrosc 2017;117:434.
[41] Onyeaju MC, Idiodi JOA, Ikot AN, Solaimani M, Hassanabadi H. J Opt 46:254.
[42] Edet CO, Al EB, Ungan F, Ali N, Rusli N, Aljunid SA, et al. Nanomaterials 2022;12:2741.
[43] Edet CO, Mahmoud S, Inyang EP, Ali N, Aljunid SA, Endut R, et al. Mathematics 2022;10:2824.
[44] Edet CO, Ikot AN. J Low Temp Phys 2021;203:84.
[45] Edet CO, Ettah EB, Aljunid SA, Endut R, Ali N, Ikot AN, et al. Symmetry 2022;14:976.
[46] Edet CO, Nwbabuzor PO, Ettah EB, Duque CA, Ali N, Ikot AN, et al. Results Phys 2022;39:105749.
[47] Edet CO, Amadi PO, Ettah EB, Ali N, Asjad M, Ikot AN. Mol Phys 2022;120:e2059025.
[48] Edet CO, Lima FCE, Almeida CAS, Ali N, Asjad M. Entropy 2022;24:1059.
[49] Edet CO, Osang JE, Ali N, Agbo EP, Aljunid SA, Endut R, et al. Quantum Rep 2022;4:238.
[50] Edet CO, Al EB, Ungan F, Ali N, Rusli N, Aljunid SA, et al. Nanomaterials 2022;12:2741.
[51] Edet CO, Khordad R, Ettah EB, Aljunid SA, Endut R, Ali N, et al. Sci Rep 2002;12:1.